Engineering Geology, 13 (1979) 111—124

THE EFFECT OF ITERATION FREQUENCY ON A NUMERICAL MODEL OF NEAR-SURFACE ICE SEGREGATION

SAMUEL I. OUTCALT

Department of Geography, University of Michigan, Ann Arbor, Mich. 48109 (U.S.A.)

(Received June 15, 1978)

ABSTRACT

Outcalt, S., 1979. The effect of iteration frequency on a numerical model of near-surface ice segregation. Eng. Geol., 13: 111—124.

It is possible to construct numerical models of the ice segregation process. However, the model is a discrete approximation of a nonlinear continuous process and thus is subject to somewhat more pronounced effects of node geometry and calculation frequency than linear models. The model more closely simulates natural frozen soil structure when vapor phase transport is included in the model structure. An iteration frequency of 10 s appeared sufficient to yield realistic results with the exponentially spaced node geometry employed in these tests.

INTRODUCTION

Ice segregation is the increase of soil ice content produced by the migration and freezing of water moving from the unfrozen to the freezing region of the soil. In an earlier paper, the effect of the addition of vapor diffusion on a model of night frost events was described in detail [1]. The intent of this paper is to examine the influence of the iteration frequency on the behavior of that numerical model. The results described in the earlier paper were achieved using an iteration step length of 60 s in the simulation of three serial night frost events in an environment similar to that of Vancouver, Canada, in mid-February. As the equations describing the diffusion of soil-water potential, temperature and water vapor are parabolic, nonlinear, cross-coupled partial differential equations, an increase in the iteration frequency (decreased interval between calculations) should produce more accurate results. The parabolic equations are solved using a fully implicit finite difference scheme involving the solution of a tridiagonal matrix of new values for the temperature, water potential and water vapor density at the computation nodes. These new values are augmented by linear equations abstracting the effects of internal distillation—evaporation and heat advected by moving soil water. The model was coupled at the surface to a surface energy—water budget model which simultaneously generated and was modulated by surface temperature and water content regimes. Thus, the

TABLE I

Components of the freezing soil system

	Notation (units)
System state variables	
Temperature, pressure (head), elevation	T (°C), H (cm water), Z (cm)
Vol. fractions (soil, water, ice, air)	X_s, X_w, X_i, X_a
System properties	
Thermal and hydraulic conductivity	K_h, K_w
Vol. heat and water capacity	C_h, C_w
System boundary conditions	
T, H at the soil surface	controlled by meteorological conditions and near-surface system state variables.
T, H at depth (water table or thermal damping depth)	constant value below water table for head . . . deepest temperature held const.
System parameters	
Empirical parameters for equations	A_x, B_x desorption curve
Used to compute system properties	A_k, B_k unsaturated
From system state variables	hydraulic cond.

diurnal surface heating and evaporation cycle was simulated, producing a transient interactive upper boundary condition. Before continuing with the analysis of iteration frequency effects, sections of the previous paper will be used to familiarize the reader with the model structure and the simulation environment.

THE FREEZING SOIL SYSTEM

The soil freezing system component structure is abstracted in Table I. The equations which govern temperature and soil water head diffusion are presented as eqs.1 and 2. Here C is the volumetric heat capacity of pure water, and the soil water head is corrected for the gravity potential before each solution:

$$\partial T/\partial t = (1/C_h)\,[\partial(K_h(\partial T/\partial Z)/\partial Z)] + (C/C_h)X_w K_w\,(\partial H/\partial Z)\,(\partial T/\partial Z)$$
(thermal diffusion + water-advected heat) (1)

$$\partial H/\partial t = (1/C_w)\,[\partial(K_w(\partial H/\partial Z)/\partial Z)] \quad \text{(soil-water head diffusion)} \tag{2}$$

The system capacities and conductivities are calculated by fitting a log-log curve to desorption data (head, water content fraction) and to unsaturated hydraulic conductivity data (conductivity, water volume fraction) and using the resulting system parameters (A_x, B_x, A_k, B_k) to update the system state variables which are needed to evaluate these system properties. The initial set of relationships employing system parameters (A_x, B_x, A_k, B_k) are presented as eqs.3—7.

$$H = A_x X_w^{B_x} \quad \text{(head as a function of } X_w,\ T \geqslant 0) \tag{3}$$

$H = W_f\, 12.46 \times 10^3\, T$ (head as a function of T, $T < 0$) (4)

$W_f = 0.42 X_i + 1.00(1 - X_i)$ (interfacial energy weighting function used in eq.4) (5)

$K_w = A_k X_w^{Bk}$ (unsaturated hydraulic conductivity as a function of the water volume fraction) (6)

$X_w = |H/A_x|^{(1/Bx)}$ (reciprocal relationship to eq.3) (7)

At subfreezing temperatures, the ratio of interfacial energy between air—water and ice—water interfaces is 0.42. Therefore, the water content at subfreezing temperatures in the region controlled by ice—water interfaces must be 2.2 times that of the water content of the surrounding soil. For this reason, the rather arbitrary weighting function (eq.5) was employed rather than the assumption that all interfaces are ice—water which produce a water content step across the freezing point. The thermal conductivity is dependent upon the individual volume fraction thermal conductivities λ_n in a truncated version of the model employed by Philip and DeVries [2]. A shape factor S_n, which in the complete model is dependent on material geometry, is calculated for each material, the material subscript index n indicating (1) mineral soil, (2) water, (3) ice, (4) air. This index system is used in this text interchangeably with the alphabetic index system already introduced. Eqs.8 and 9 are employed to calculate the bulk soil thermal conductivity. The model assumes that the contribution of an individual material species (volume fraction) to the species shape weighting factor must be proportional to the thermal gradient in the material (inversely proportional to the thermal conductivity species) and the volume fraction of the species as a product which is normalized:

$$S_n = (X_n/\lambda_n) / \sum_{k=1}^{4} (X_k/\lambda_k) \tag{8}$$

$$K_h = \sum_{n=1}^{4} S_n X_n \lambda_n / \sum_{k=1}^{4} S_k X_k \tag{9}$$

The system capacities can also be calculated on the basis of system parameters and state variables as demonstrated by eqs.10—13, where L_f is the latent heat of fusion and p_w is the density of water.

$C_w = (\partial H/\partial X_w)^{-1}$ (vol. capacity for water) (10)

$\partial H/\partial X_w = A_x B_x X_w^{(B_x - 1)}$ (first derivative of desorption curve) (11)

$C_h = 0.46 X_s + X_w + 0.5 X_i + p_w L_f \partial X_w/\partial T$ (vol. heat capacity + fusion effects) (12)

$\partial X_w/\partial T = (\partial X_w/\partial H)\,(\partial H/\partial T)$

where $\partial H/\partial T = 12.46 \times 10^3$ cm °C^{-1}.

The change in the unfrozen water content below freezing is ΔX_w. From this value, the volumetric change in ice content ΔX_i can be calculated, and

a new ice content volume fraction is estimated using eqs.13—15. This operation follows each updating of the unfrozen water content, using eq.7:

$$\Delta X_i = -\Delta X_w/0.92 \quad \text{(change in ice vol. fraction)} \tag{13}$$

$$X_w = X_w + \Delta X_w \quad \text{(new water vol. fraction)} \tag{14}$$

$$X_i = X_i + \Delta X_i \quad \text{(new ice vol. fraction)} \tag{15}$$

Note that in the previous set of equations, the change in water volume fraction ΔX_w is the change in unfrozen water content from the previous equilibrium condition, including water movement. Excess or deficient water is added or withdrawn from the ice volume fraction to meet current equilibrium conditions. This is the section of model which initiates the ice segregation process under conditions when excess water is accumulating at computation locations. If the system is above freezing the ice content is nil and the water content is calculated using eq.7, after a cycle of water movement has been computed. The air volume fraction is calculated using eq.16:

$$X_a = X_p - X_w \quad \text{(air vol. fraction)} \tag{16}$$

where X_p is the initial porosity.

In the freezing environment the air content is unaltered, but the volume fractions at a computation location are normalized for each material species (X_n) as illustrated in eq.17:

$$X_n = X_n / \sum_{k=1}^{4} X_k \qquad (n = 1, 2, 3, 4) \tag{17}$$

The heave (hev) or displacement of the original internode (nodes are computation locations) spacing is set at unity at above-freezing temperatures. In the frost system the heave is defined by the ratio of the sum of the ice, air and water volume fractions to the original unfrozen porosity of the soil:

$$\text{hev} = \frac{1 - X_p}{1 - X_w - X_i - X_a} \tag{18}$$

The original space vector is developed using an unequal node spacing rule where $-Z(L)$ is the depth at computation node L and $DZ(L)$ is the initial (unfrozen) difference in depth between nodes L and $L-1$. When the node vector is originally set, the following conventions are used.

$$Z(1) = 0.00 \quad \text{(elevation of top node)} \tag{19}$$

$$DZ(1) = 0.00 \quad \text{(first spacing difference)} \tag{20}$$

Any rule may be used to specify each $DZ(L)$. Here we used an exponential spacing (cm):

$$DZ(L) = 0.2 \exp[(L-1)/10] \qquad (L = 2, 3, 4, \ldots \text{last}) \tag{21}$$

Displacement of the nodes in the soil vector during segregation ice growth and ablation is accomplished by the following operation:

$$Z(L-1) = Z(L) + DZ(L)\ [\ \mathrm{hev}(L) + \mathrm{hev}(L-1)]/2) \qquad (L = 2, 3, 4, \ldots \text{last}) \qquad (22)$$

Some investigators [3, 4] have stressed the importance of heat advected by water flow, and these effects are included in the simple model described above. Two recent articles [5, 6] indicate the problems encountered in building and testing soil models which include vapor phase transport and internal distillation effects in an above-freezing environment. As stated previously, the object of this paper is to examine the effects of the addition of the vapor phase to a simple model of coupled heat and mass transfer in freezing soils. In the following, the mechanism for adding an interactive upper boundary condition will be briefly described.

THE OPERATION OF THE SIMPLE SOIL MODEL

The soil model consists of two primary parts. Firstly, there are a set of routines which use current values of soil water head and temperature to update the volume fractions and system properties with the aid of empirical equations containing the system parameters. Secondly, an implicit numerical routine which simulates the diffusion of heat and soil water head in the simple version, and water vapor diffusion in the extended model. These procedures are discussed at length and in detail in previous publications [7, 8]. The algorithm employed can handle extreme conditions of strong flux divergence in the vicinity of a computation node. This feature is extremely helpful due to the strong contrast in system properties in the vicinity of the ice point and ice lenses.

The surface energy budget is simulated using an equilibrium temperature algorithm which is quite simple and efficient [9]. In this model, a generated diurnal regime of solar radiation drives the evolution of the system. The surface temperature is first solved for a specific set of system boundary conditions (latitude; month; day; mean daily air temperature, humidity, wind speed, pressure; surface roughness; wet—dry albedo; precipitable water; dust content; radiant temperature of the sky hemisphere) and the initial temperature field in the soil, as well as the soil system parameters described previously. The solution of the surface temperature is achieved by the application of the secant algorithm (in this application, identical to Newton—Raphson) to an energy budget equation transcendental in surface temperature. Once the surface temperature is known, the soil water head at the surface (node 1) is updated using eqs.23 and 24, where $H(1)$ is the head at the surface and $H(2)$ is the head at the first subsurface node. In the first of these equations, E is the evaporative flux to the atmosphere.

$$H(1) = H(2) + (E/C_0) \quad \text{(calculates head at surface)} \qquad (23)$$

$$C_0 = [\tfrac{1}{2}(K_w(1) + K_w(2))]/|Z(2) - Z(1)| \qquad (24)$$

The surface relative humidity fraction (SRHF) is then adjusted to the current value of the soil water head by means of the Gibbs free energy expression:

$$\text{SRHF} = \exp\left[(gH(1))/(R(T(1) + 273.16))\right] \tag{25}$$

where g is the gravitational const. and R is the gas const. The components of the surface energy budget are therefore strongly modulated by the state of the coupled soil heat—water system.

THE VAPOR PHASE

Two versions of the model were used in the simulation trial which follows. The first model, described in the preceding section, includes the effects of coupled heat and water flow with heat advection by water movement. The second version contains an additional subroutine to simulate the effects of vapor diffusion and internal distillation on the soil water and temperature fields, as well as the segregation of ice at subfreezing temperatures. It is probable that vapor diffusion effects are significant in the zone near the freezing front if the analogy between the desiccating effects of an evaporating front and a freezing front is valid. The expanded model employs a value for the diffusivity of water vapor which follows Philip and DeVries [2] in which D_{atm} is the molecular diffusivity of water vapor in air, α is a tortuosity factor, a is the volume fraction of air and ν is a mass flow factor. The values used in eq.26 were those of Philip and DeVries [2]:

$$D_{\text{v}} = D_{\text{atm}}\alpha a\nu \tag{26}$$

The diffusion of the vapor phase was calculated using the same numerical algorithms employed in the diffusion of temperature and soil water head. These methods were used to provide solutions to eq.27, which is a parabolic partial differential equation with the same structure as the equations describing temperature and head diffusion:

$$\partial V/\partial t = D_{\text{v}}\partial^2 V/\partial Z^2 \tag{27}$$

where V is water vapor density (g/cm^3), another state variable.

The model computes vapor, temperature and head diffusion in that order. The equilibrium vapor density at an internal node is a function of temperature, air pressure and soil water head (potential). The state variables T, H are continually changing at the near-surface nodes during a diurnal cycle. Thus, it is likely that the value of vapor density resulting from diffusion in the three diffusing subsystems (temperature, potential, vapor), which is labeled V_1, will be different from the current equilibrium value demanded by the state variables V_2. This difference (ΔV) represents a nonequilibrium condition that must be adjusted by internal distillation or evaporation at a node. In modeling this process, the action here is abstracted as a lateral adjustment compared to diffusion and advection which are vertical acting processes. The process is confined to a computation node:

$$\Delta V = V_2 - V_1 \quad \text{(disequilibrium in vapor density at a computation node)} \tag{28}$$

The difference, if positive, must be balanced by local evaporation from the water volume fraction in a discrete model of a continuous process:

$$\Delta V = \text{evap} \cdot \rho_w \tag{29}$$

where evap is local evaporation and ρ_w the density of water. Further adjustments are carried out on the volume fractions at a computation node:

$$X_\epsilon = X_w + X_a \quad \text{(sum of initial air + water fractions)} \tag{30}$$

$$X_w = X_w - \text{evap} \quad \text{(adjust. water vol. fraction)} \tag{31}$$

$$X_a = X_\epsilon - X_w \quad \text{(adjust. air vol. fraction)} \tag{32}$$

Internal distillation (negative evaporation) or evaporation must accompany these changes in phase and influence the temperature field through latent heat effects. Therefore, it is necessary to adjust the node temperatures for these effects:

$$\Delta T = -\text{evap}\,(\mathcal{L}/C_h) \tag{33}$$

where $\mathcal{L}$ is temperature-dependent latent heat.

$$T = T + \Delta T \tag{34}$$

The water vapor flux to the upper boundary node is estimated using eq.35:

$$V(1) = V(1) + D_v(\partial V/\partial Z)\Delta t \tag{35}$$

This model structure is extremely simple and is designed to offer only a basic framework for more elaborate efforts and a primitive evaluation of the impact of vapor diffusion on the response of initially nearly saturated soil-water systems to frost.

THE SIMULATION ENVIRONMENT

The simulator was run in a manner which attempted to match the environment of 11 consecutive needle ice events which occurred at Vancouver, British Columbia during February 1968 [10]. The input data used is listed in Table II. The comparison of some simulated and observed environmental variables is given in Table III.

It will be noted that the needle ice height in the two models is two to three times larger than in the field observations. This difference is probably the result of simulating a clear sky in the model when there was partial cloud cover during the field observation period. In addition, the model does not simulate undercooling before nucleation and thus lengthens the time available for needle growth. The discrepancy in the maximum value of net radiation is probably the result of the assumption in the model of clear sky. However, the discrepancy is only of the order of 10—15%, which is

TABLE II

Simulation input data

Latitude	40.3°
Month	2.0
Day	15.0
Air temp.*	7.0°C
Wind vel.	120.0 cm s^{-1}
Station pressure	1020.0 mb
Relative humidity	55.0%
Roughness length	2.0 cm
Dry albedo	0.25
Wet albedo	0.15
Atm. precipitable water	7.0 mm
Atm. dust	0.2 particles cm^{-3}
Sky radiation temp.	−18.0°C
Water table elevation	−5.0 cm
Initial soil temp.	7.0°C
Soil parameters	
Porosity	0.38
A_x	157 E-7
B_x	−11.434
A_k	1.366
B_k	9.852

*All weather variables are daily means.

TABLE III

Comparison of field and simulated environments

Variable	Field range*[1]	Simple model*[2]	Vapor model
Maximum needle height (cm)	0.46 — 1.20	2.20	3.10
Max. surface temp. (°C)	13.6 — 10.9	14.0	12.7
Max. net radiation (mly/min)	340 — 375	321	316

*[1] *Field range* from 11-day event series commencing 6 Feb. 1968, Vancouver.
*[2] *Model values* from simulations during second day.

within the realm of precision of a polythene-shielded net radiometer. Lastly, the modeled maximum daily surface temperature is well within the range of observations. Thus, the simulated environment is intended to match a February diurnal frost event in coastal southern British Columbia.

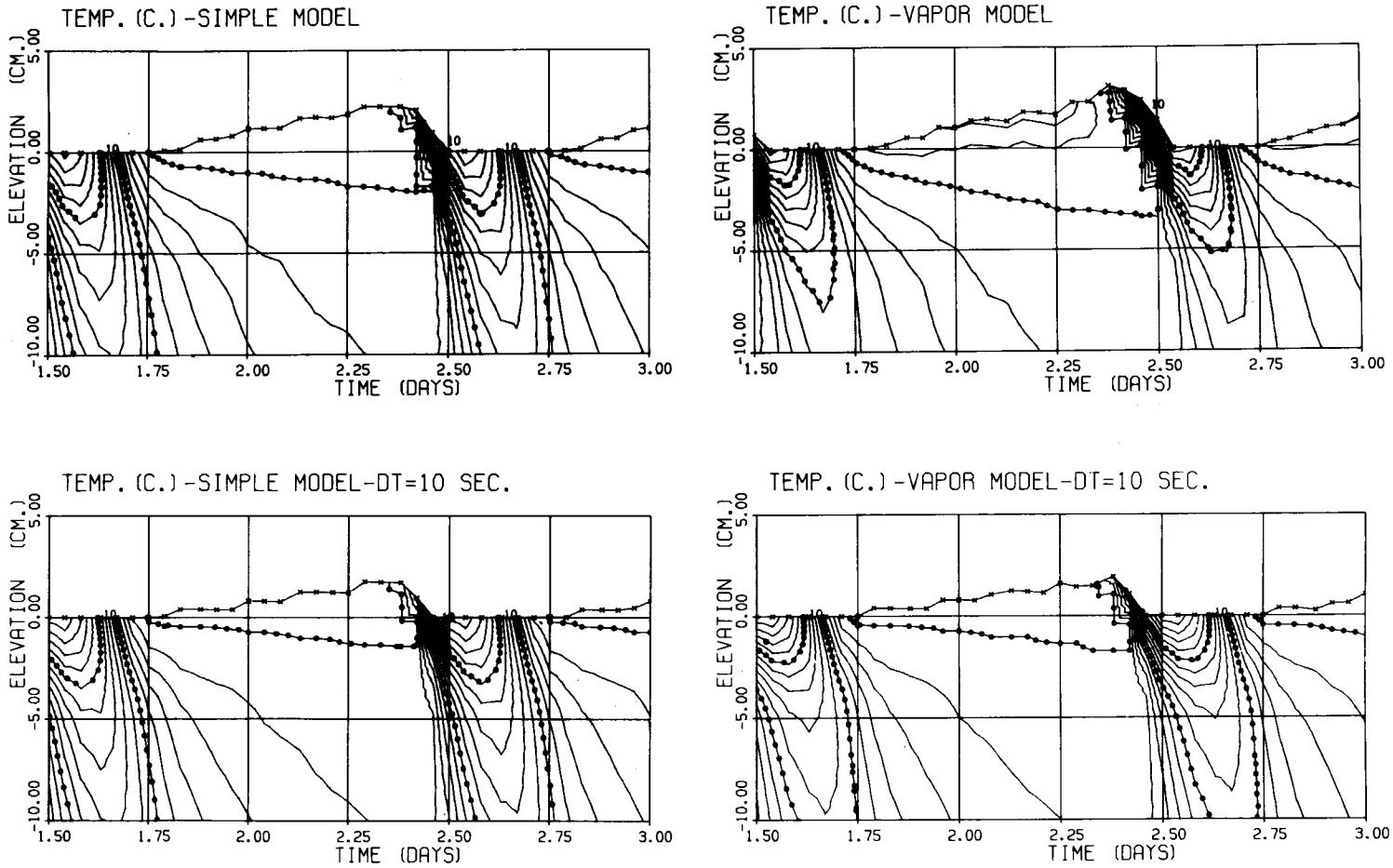

Fig.1. The effect of the iteration frequency on the thermal regime. Note that in both the vapor and simple models, the rate and total depth of frost penetration is reduced by increasing the iteration frequency. The index isotherm of 0°C is the only index contour on the 2.25-day time line. The contour interval is 1°C.

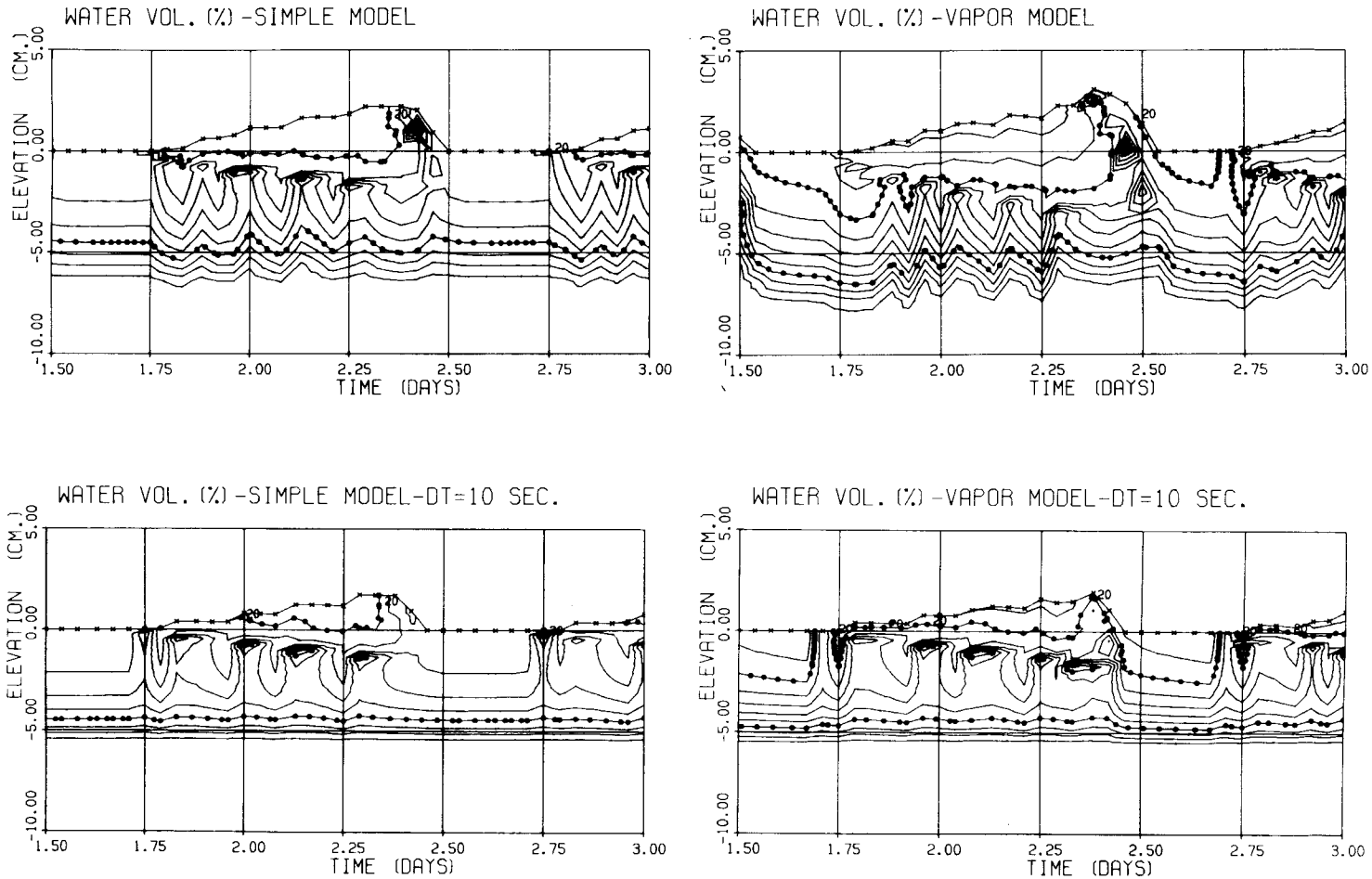

Fig.2. The effect of iteration frequency on the water content regime. The lowest index contour is 30% with water volume generally decreasing toward the surface except for the water content lull produced by melt. Note that the depth of penetration of the quasi-periodic ridges and troughs is reduced by an increased iteration frequency in both models, the effect on the vapor model being most pronounced. The contour interval is 2%.

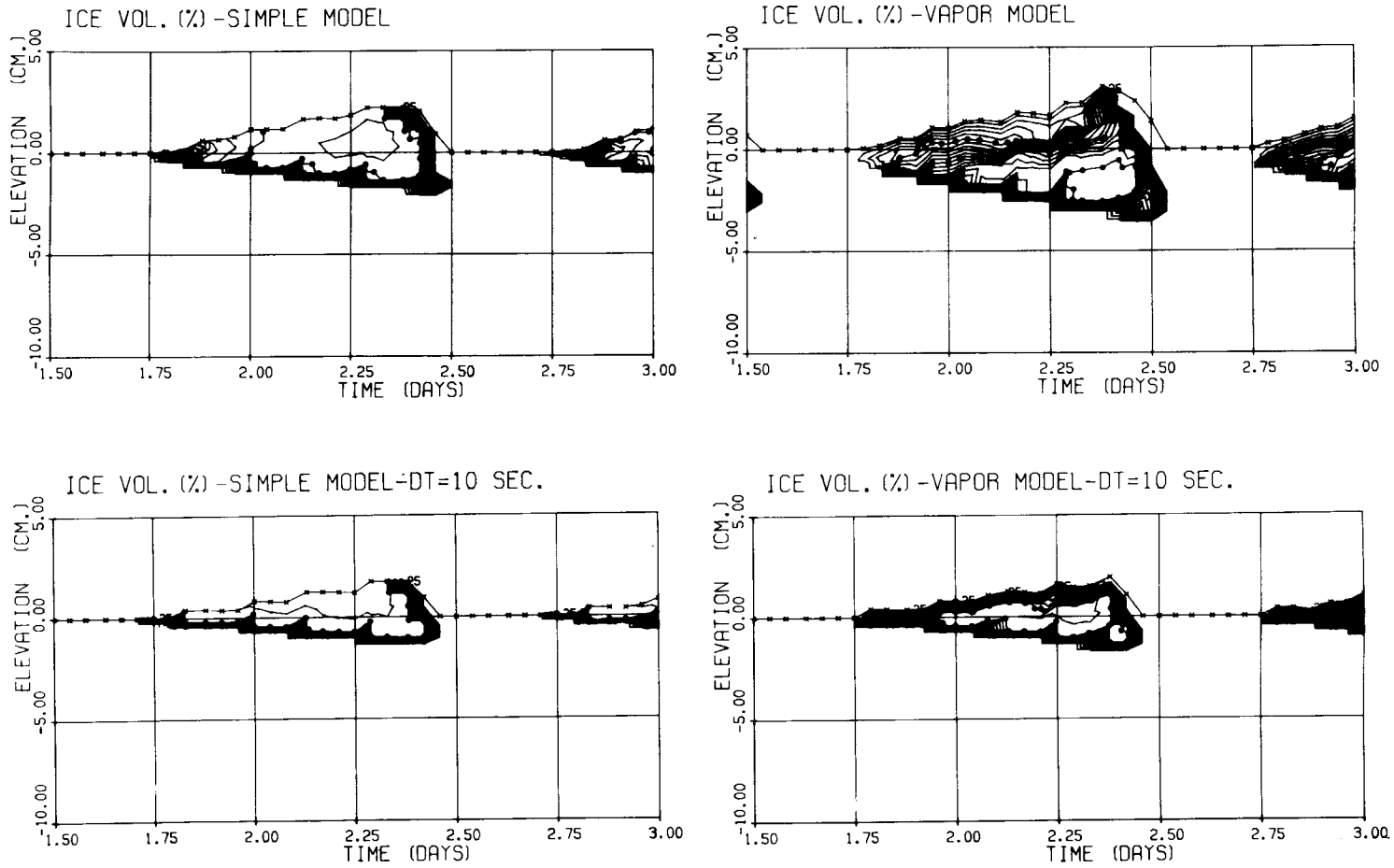

Fig.3. The effect of iteration frequency on ice content. As previously noted, the increased iteration frequency reduces the depth of frost penetration. The high frequency vapor model produces a decrease in the cap depth and desiccation in terms of both water and ice within the cap region. The contour interval is 5%.

THE EFFECTS OF THE VARIABLE TIME STEP ON SIMPLE AND VAPOR MODELS

The original node depth for the first 18 computation nodes were 0.0, 0.22, 0.46, 0.73, 1.03, 1.36, 1.73, 2.13, 2.58, 3.07, 3.61, 4.21, 4.88, 5.61, 6.72, 7.32, 8.31 and 9.40 cm. These values of temperature water and ice content by volume were mapped during the second event on a time–depth grid. The simple and vapor models were run using time steps of 60 and 10 s to explore the effects of time step length as the node response. These materials are presented as Figs.1–3.

Examination of Figs.1–3 demonstrates that the ice segregation process is extremely sensitive to model iteration frequency. The effect is most pronounced in the vapor model, due presumably to the relatively high diffusivity of water vapor. It is important to note that water vapor diffusion in an extremely wet soil appears strongly to modulate the structure of the frozen zone.

The high-frequency vapor model was run with the water table depth increased to 150 cm, the resulting diagrams being shown as Figs.4–6. It is interesting to note that in the drier soil the diurnal effects of ice growth-melt and quasi-periodic phenomena are extremely weak at depths greater than 10 cm.

CONCLUSIONS

The use of high iteration frequencies (10 s) seems to produce a more realistic simulation of needle ice events than the lower frequency models.

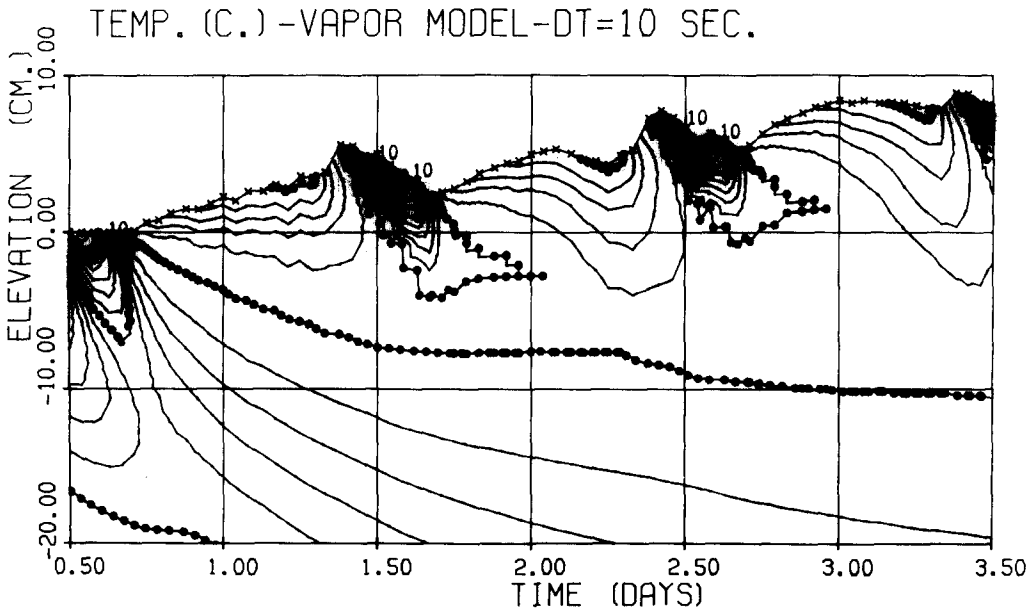

Fig.4. The thermal regime of the high-frequency vapor model with the water table depth increased to 150 cm.

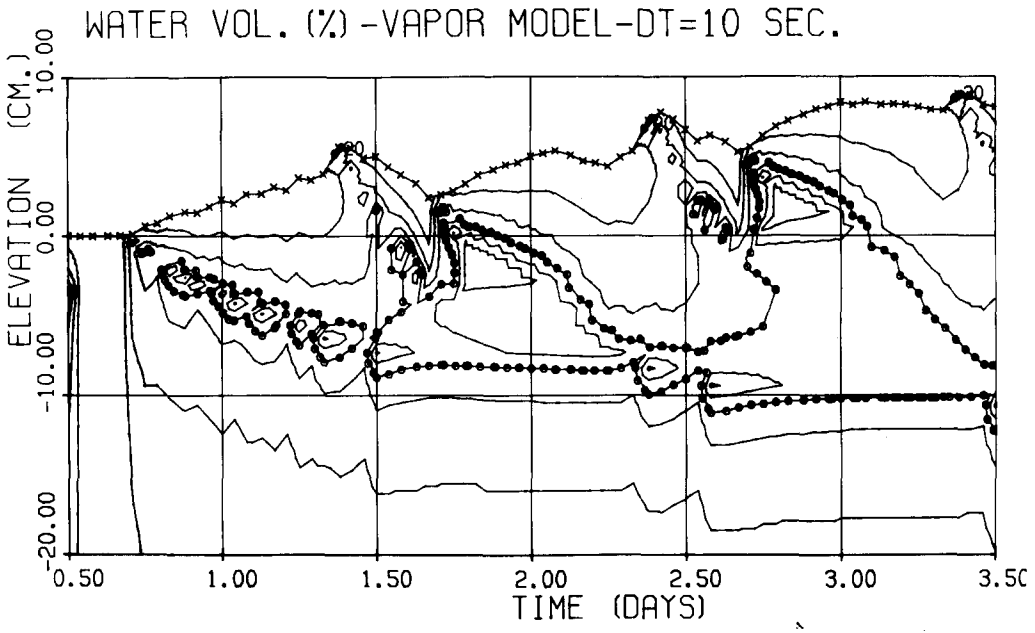

Fig.5. The water content regime with the water table elevation of —150 cm.

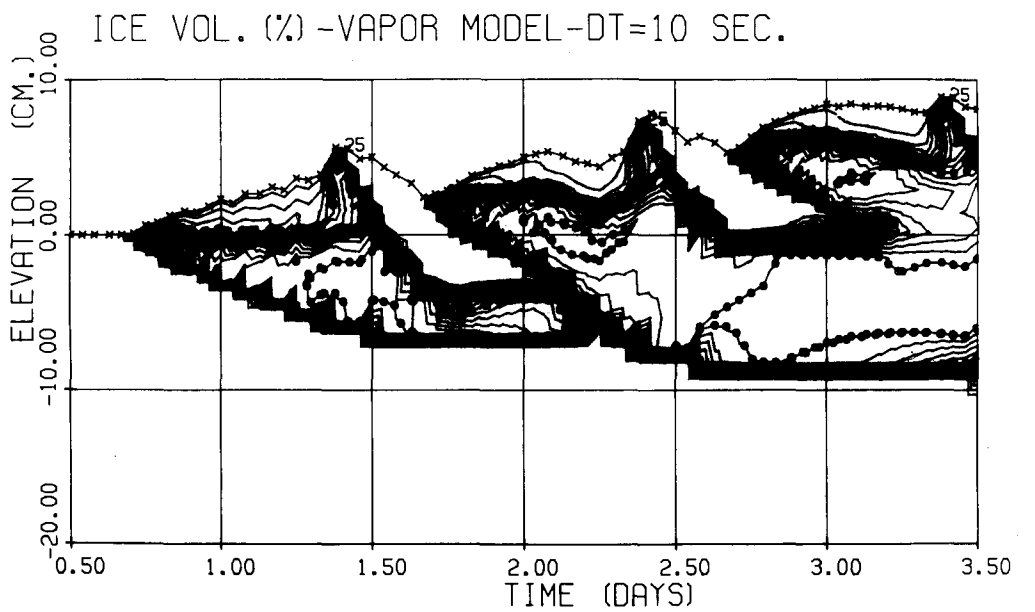

Fig.6. The ice content regime with the water table elevation set at —150 cm.

The effect is believed to be a product of the nonlinear cross-coupled nature of the model-defining equations and the incorporation of linear equations in the model structure. The fact that vapor diffusion is a significant process in wet soil in the vicinity of the freezing plane cannot be overemphasized. Thus, the analogy of internal evaporation—distillation in freezing and evaporating soils seems useful. It should be recalled that these statements are restricted to the conditions of the simulated environment. Future modeling research should be directed towards the influence of the vapor phase in the freezing of initially wet soils over much longer periods (years, decades). The apparent mobility of water in both the vapor and liquid phases at subfreezing temperatures is significant in the design of cold buried natural gas transmission lines and storage facilities when the surrounding soil temperature is artificially reduced.

ACKNOWLEDGEMENTS

The author's enthusiasm for this topic has been maintained by frequent contacts with a truly international community of scientists interested in frost problems. These contacts were made possible by the U.S. National Science Foundation.

REFERENCES

1 Outcalt, S., 1977. The influence of the addition of water vapor diffusion on the numerical simulation of the process of ice segregation. Frost i Jord, Oslo (manuscript in review, June 1977).
2 Philip, J.R. and Devries, D.A., 1957. Moisture movement in porous material under temperature gradients. Trans. Am. Geophys. Union, 38(2): 222—232.
3 Kinosita, S., 1973. Water migration in soil during frost heaving. In: Proc. 2nd Int. Conf. on Permafrost. Yakutsk Publ. House, Ya. A.S.S.R., Vol.1, pp.68—72.
4 Outcalt, S., 1971. Field observations of soil temperature and water tension feedback effects on needle ice nights. Arch. Meteorol. Geophys. Bioklimatol., A20: 43—53.
5 Jackson, R.D., Reginato, R.J., Kimball, B.A. and Nakyama, F.S., 1974. Diurnal soil-water evaporation: comparison of measured and calculated soil-water fluxes, Soil Sci. Soc. Am. Proc., 38(6): 861—866.
6 Jackson, R.D., Reginato, R.J., Kimball, B.A., Idso, S.B. and Nakyama, F.S., 1975. Heat and water transfer in a natural soil environment. In: D.A. Devries and R. Afgan (Editors), Heat and Mass Transfer in the Biosphere. Scripta, Washington, D.C.
7 Outcalt, S. and Carlson, J., 1975. A coupled soil thermal regime surface energy budget simulator. Proc. Conf. on Soil-water Problems in Cold Regions, Special Task Force, Div. Hydrol., Am. Geophys. Union, 6—7 May 1975, Calgary, pp.1—20.
8 Carlson, J.H. and Outcalt, S., 1975. The integrated simulation of soil heat-water flow, ice segregation and surface energy transfer regime. In: A. Dybbs (Editor), Proc. Workshop on Heat and Mass Transfer in Porous Media, Oct. 14—15, 1974, sponsored by N.S.F. and Case Western Reserve Univ., pp.207—211.
9 Outcalt, S., 1972. The development and application of a simple digital surface climate simulator. J. Appl., Meteorol., 11(4): 629—636.
10 Outcalt, S., 1970. A study of time dependence during serial needle ice events. Arch. Meteorol. Geophys. Bioklimatol., A19: 329—337.